Sensors and Actuators B, 11 (1993) 9–19

Gas sensors using correlation spectroscopy compatible with fibre-optic operation*

H. O. Edwards and J. P. Dakin
Optoelectronics Research Centre, University of Southampton, Southampton SO9 5NH (UK)

Abstract

This paper reviews methods for gas detection using real-time correlation spectroscopy. These methods involve using a gas sample in a reference cell as a matched optical filter to detect, preferentially, similar absorption spectra in a measurement cell. The methods all have the advantage of excellent selectivity, even using broadband sources, and are suitable for remote detection over optical-fibre leads. Our previously published methods using pressure and Stark modulation are reviewed. In addition, our recent theoretical treatment of the methods is presented. Finally, we describe new atmospheric-pressure measurements of gases using the method of phase-modulation spectroscopy.

Introduction

Many common gases of industrial and environmental importance exhibit their fundamental optical absorption bands in the infrared region. Weaker overtone bands extend into the near infrared and visible region, thus coinciding with the low-loss transmission window for silica fibre. Absorption in these regions is usually due to transitions between vibrational–rotational energy levels of the molecule. As the fine-line structure within an absorption band is highly specific to the gas species, recognition of these features provides for highly selective gas detection. The band positions of a selection of common gases are shown in simple form in Fig. 1, together with the absorption spectrum of silica optical fibre. Infrared fibres, typically manufactured from fluoride glasses, are also available with acceptable loss at wavelengths up to 5 μm. These fibres make the stronger fundamental gas absorptions accessible, thereby enhancing the potential detection sensitivity, but have a much higher cost and are not so mechanically robust.

The low loss of silica optical fibres allows a gas-sampling cell to be located many kilometres from the monitoring station with little degradation of the signal. The passive nature of the sensor head and the low optical power used make such optical techniques inherently safe for hazardous applications, such as the monitoring of explosive gases [1, 2].

Early fibre-optic-based methods measured gas transmission using broadband and LED sources [3] and thus had poor selectivity. Other recent methods have used laser sources [4], but these can present problems due to the long coherence length, in particular, modal noise effects in multimode fibre. Even when single-mode fibre is used to prevent this, effects such as Fabry–Perot etalons at connectors, and more complex interference patterns within the measurement cell and launch optics, can potentially cause severe practical limitations. Correlation spectroscopy allows the use of a broadband source, yet still makes use of the fine spectral features of the gas spectrum. It has the further advantage of employing all of the spectral information contained in the selected gas-absorption band.

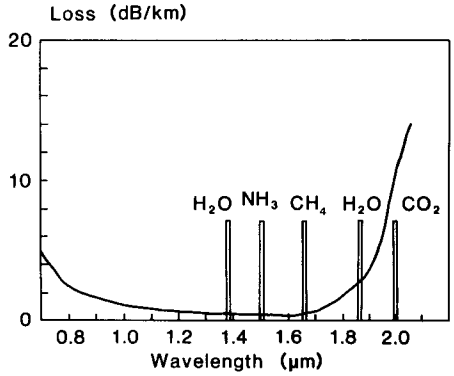

Fig. 1. Absorption bands of some common gases within the transmission window for silica fibre.

The basic methods of real-time correlation spectrometry all involve modulation of the absorption spectrum of the reference gas sample, relative to the gas to be measured. Modulation can be achieved directly by varying the absorption spectrum of the reference gas. In this paper, we review progress with three modulation techniques, each using the correlation spectroscopy method. These include Stark, pressure and phase modulation.

*Plenary paper.

A common optical configuration was adopted for all of the schemes investigated in this study, as shown schematically in Fig. 2(a) and (b). The apparatus comprises two gas cells, through which light from a broadband source is passed sequentially, prior to detection. In our fibre-remoted version, light is conveyed to the cells via multimode optical fibre, and a bandpass filter is included (preferably before the detector) in order to attenuate light outside the absorption band of the relevant gas. The gas to be detected is introduced into the measurement cell, whereas the reference cell is filled to a known concentration of the gas to be detected and then sealed.

Modulation of the absorption spectrum of either gas cell results in a change in the correlation between the spectrum of the measurement gas sample and the reference gas, thereby causing a variation in the transmission of the system. The absorption spectrum of the gas contained in the reference cell may be modulated, either directly or indirectly, in order to produce the desired signal. The synchronously detected output signal then depends on the concentration of the correlating gas in the measurement cell. Modulation methods that act directly on the gas include Stark and pressure modulation, as depicted in Fig. 2(a).

Stark modulation of gases occurs only with polar molecules and results from the splitting (or broadening at atmospheric pressure) of individual absorption lines when a large electric field is applied. The pressure-modulation technique is more generally applicable. This involves periodically pressurizing the gas within the reference cell, causing a variation in both the strength and width of the absorption lines.

A third modulation approach is indirect and involves a redistribution of the optical spectrum of the light as it passes between the measurement and the reference cell, as shown schematically in Fig. 2(b). Angle modulation of the light (using phase or frequency modulation) is a means of achieving this. We shall present both measurements and theoretical results for this method.

It should be emphasized that although these modulation techniques appear to be alternative technologies, they each have their own particular advantages depending on the gas species, sensitivity requirements and cost constraints for the system. The three methods are described below in more detail.

Pressure-modulation gas detection

Pressure-modulation spectroscopy involves applying a periodic pressure fluctuation to the reference gas cell to modulate its absorption. A schematic diagram of the arrangement is shown in Fig. 3. An optical bandpass filter is included, preferably before the optical receiver, in order to select the relevant absorption band of the gas to be detected.

The first (bulk-optical) pressure-modulation scheme for correlation spectroscopy was originally proposed by Goody [5], and further exploited by Taylor *et al.* [6] for atmospheric and planetary measurements. A reciprocating piston compressor was used to modulate the gas pressure. The technique has received little attention for quantitative terrestrial gas sensing, despite having a number of potential advantages for this application. These include excellent selectivity to the desired gas, a

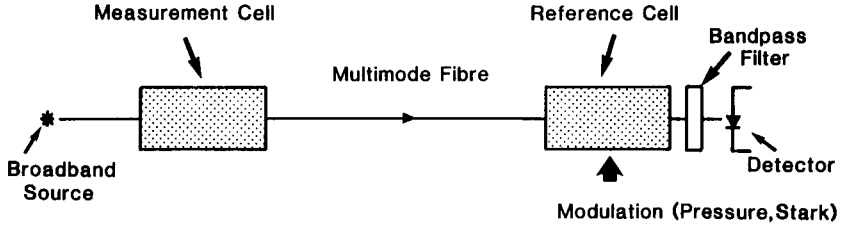

(a)

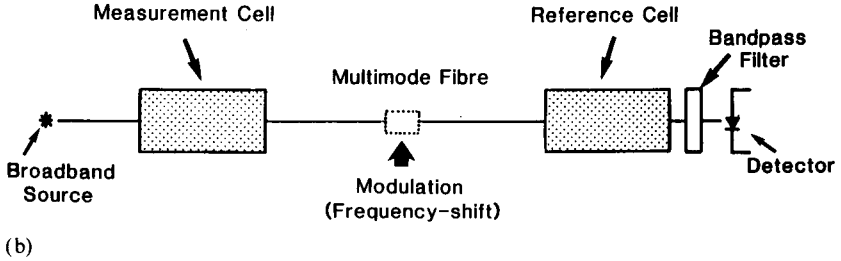

(b)

Fig. 2. Schematic diagram for the correlation spectroscopy scheme: (a) pressure and Stark modulation; (b) angle modulation.

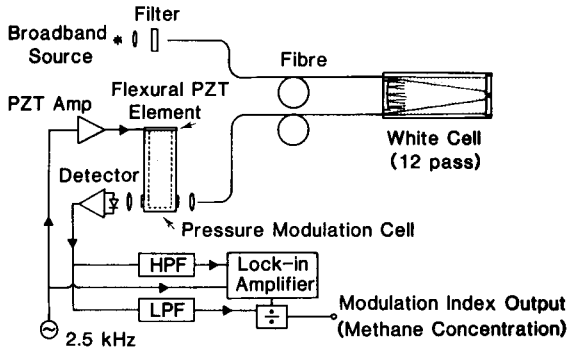

Fig. 3. Experimental configuration for the pressure-modulated methane detector.

modulated signal format and a good gas-detection sensitivity. The reason for little development of the method for industrial sensing is probably the high cost of the precision modulation cells used in these systems. The pressure-modulation principle has been further developed in our work to include a fibre-remoted sensor head and an improved pressure modulator [7].

Analysis of the pressure-modulated gas detector

The pressure modulation imposes a small intensity modulation on the mean optical power level received at the detector, which can be accurately monitored using synchronous electronic post-detection techniques. As gas is introduced into the measurement cell, the amplitude of the signal reduces, enabling the concentration to be derived from the optical-modulation index of the detected signal, which is determined by dividing the alternating component of the signal by the mean level. This renders the system essentially immune to slow fluctuations in the source intensity or in the attenuation of the optical system.

If the two gases are of the same species, and hence correlate, light is selectively absorbed by the gas in the measurement cell before the beam enters the reference cell. Light is only removed in the specific spectral regions that undergo the modulation in absorption in the reference cell. Hence, the modulation index of the detected signal diminishes with increasing gas concentration in the measurement cell.

For an uncorrelated gas line having negligible spectral overlap with the reference gas, only the mean optical level is affected, but to a very small degree due to the narrow linewidth of typical lines. Hence, the amplitude of the alternating signal is essentially unaffected. This accounts for the excellent cross-sensitivity performance of this technique in rejecting uncorrelated gases.

For the analysis below a number of simplifying assumptions are made. An ideal 'top-hat' optical bandpass filter is assumed, which rejects all light outside the selected absorption band and has a constant transmission over the spectral region occupied by the band. The linewidths of all absorption lines are assumed to be the same within a band. The model chosen to describe the lineshape, $k(v)$, employed is that proposed by Lindholm [8]. This function describes collision broadening of a line of an absorbing molecule due to interaction with a non-absorbing diluent gas (e.g., air). Consequently, it is an excellent model for the calculation of gas/air mixtures.

An isolated gas-absorption line has a transmission, $T(v)$, given by the Beer–Lambert law for a homogeneous medium:

$$T(v) = \exp(-k(v)CL) \tag{1}$$

Optical frequency is denoted by v, C is the gas concentration and L is the path length. The variation in the width of an absorption line with temperature, pressure and gas concentration is assumed to follow the relation predicted by impact theory, where the linewidth is proportional to the product of the mean molecular speed and the gas concentration [9]. The periodic compression of the reference gas within the pressure-modulation cell occurs at audio frequencies, and so can be considered to be adiabatic [10].

The system performance was predicted by numerical integration. The integrated transmission, I, of the system can be evaluated for a number, N, of absorption lines constituting a band:

$$I = I_0 \int_{v_1}^{v_2} \prod_{i=1}^{N} [T_{1i}(v) T_{2i}(v, P)] \, dv \tag{2}$$

The absorption band is taken to extend from v_1 to v_2, and the symbol i represents the ith line of the band. The measurement cell is denoted by the subscript 1, and the reference cell by the subscript 2. The peak spectral intensity, I_0, is defined as the level detected when no gas is present in either the reference or measurement cell.

As the linewidth and concentration of the gas in the reference cell are modulated by the applied pressure fluctuations, the integrated transmission varies. The optical modulation index is calculated by dividing the peak-to-peak transmission excursions by the mean transmission. The linestrengths of corresponding lines in the measurement and reference cells are taken to be equal and the static linewidths for the individual pressure-broadened lines are assumed to be similar. The central frequencies of optical absorption lines were taken from data published by Margolis [11]. Linestrength values for our atmospheric pressure-broadened conditions were difficult to obtain, as detailed studies, such as those of Margolis, have been performed only at low pressure, where each line is resolved into a manifold of very closely spaced lines. Linestrength values were

therefore taken from a moderate resolution (6 GHz) plot kindly supplied by NPL [12], which we scaled to give a static absorption of 2.5%, as measured experimentally for our reference cell. The integrated absorption of the band as a whole, calculated by this means, agrees well with the value quoted from the HITRAN database [13]. Different linewidth values [14] are assumed for the air-broadened linewidth (3.6 GHz) in the measurement cell, compared with the self-broadened linewidth (5 GHz) of the reference cell.

Modelling was performed for the $2\nu_3$ band of methane, centred at 1.66 μm. An integration span of 65 nm was employed, covering the P, Q and R branches of the band. In order to compare results with our experimental data, we assumed a reference cell length of 3.6 cm at 1 atm (100% pure) methane, and a measurement cell of 480 cm length, containing various selected concentrations up to 3%.

Curves of the optical-modulation index against measurement cell concentration were calculated at various pressure-modulation index values (Fig. 4). The values of pressure-modulation index correspond to those measured experimentally.

Resonant acoustic cell pressure modulator

The resonant acoustic cell used for our pressure modulator was formed from a closed cylindrical cavity in a metal block, with an optical window at one end and a flexural piezoelectric element situated at the opposite end. The flexural element consisted of a piezoelectric crystal bonded onto a thin metal shim. The application of an alternating voltage to the crystal induced a hemispherical flexing of the piezoelectric crystal, and so acoustic waves were launched into the cavity containing the reference gas. The system was configured so that the mechanical resonance frequency of the piezoelectric element coincided with the primary acoustic resonance of the cell. The quality factor of the acoustic chamber was measured to be 90 in this application.

Compared with simple low-frequency piston compressors described previously, the device has the advantages of a high modulation frequency (2.5 kHz), compact size, low power consumption and simple piezoelectric excitation. The cell design is simplified in requiring no sliding seals, and has no moving parts other than the acoustic source. Although the amplitude of the pressure modulation achieved with this cell was lower than that of piston compressors used by other workers, the resonant cell has many advantages over the piston scheme, and a sensor with good performance has been realized.

Experimental results

The optical configuration and signal processing employed for our experimental investigations are shown in Fig. 3. For the first experiments, light from a tungsten broadband source was launched through an optical bandpass filter into the fibre. The filter was chosen to select the absorption band for methane at 1.66 μm, and its transmission characteristics are shown in Fig. 5, together with the absorption spectrum of methane for comparison. It can be noted that this filter does not cover the entire band, merely the P and Q branches, but was the closest commercially available example. This mismatch only affects the signal-to-noise ratio for methane detection to a small extent. However, as shown later, the cross-sensitivity results for ethane are not as good as they would be for a better matched filter, as overlap with the spectrum for ethane tends to be stronger over the filtered section of the band.

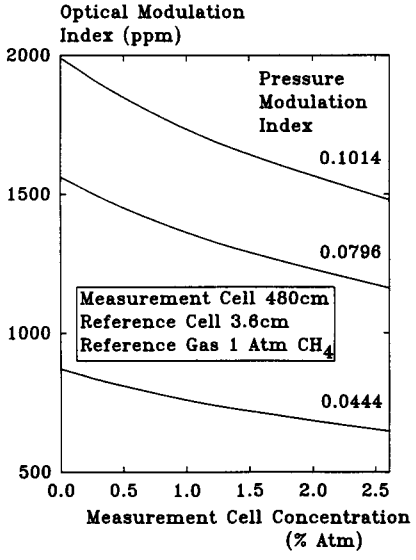

Fig. 4. Calculated optical-modulation index vs. methane concentration for the pressure-modulated scheme.

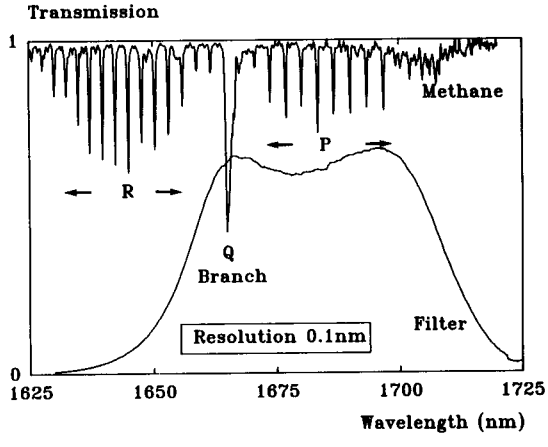

Fig. 5. Optical transmission spectrum for the $2\nu_3$ methane band (10.5 cm path length at 1 atm), and for the band selection filter.

In our first experimental demonstration [7], the measurement cell was linked to the source via a 10 m length of multimode (100/140 μm) fibre. The measurement cell was a twelve-pass White [15] cell with an effective path length of 480 cm. A fibre-to-fibre insertion loss of 9 dB was achieved with the gas cell design employed. Methane concentrations of up to 2.6% in air were measured. The reference cell had a path length of 3.6 cm and a fibre-to-fibre insertion loss of 3 dB.

Calibration of the system as a methane detector was performed by filling the measurement cell with a range of known methane/air mixtures. Measurements were made at several values of the pressure-modulation index, and the resulting variation of detected optical-modulation index is shown in Fig. 6, as a function of measurement cell concentration. As would be expected, the optical-modulation index falls as the methane concentration in the measurement cell is increased.

The measured noise level of the optical receiver corresponded to the value expected for shot noise due to the photocurrent. This value was assumed in theoretical estimations of the noise-limited gas sensitivity. The detection limit is defined as the equivalent change in methane concentration corresponding to a unity signal-to-noise ratio at the detector. For the highest pressure ratio applied, a typical received optical power of 0.25 μW and a processing time constant of 1 s, the noise-limited sensitivity was 50 ppm methane by volume, equivalent to 0.1% of the lower explosive limit.

Cross-sensitivity measurements for the methane sensor

As already mentioned, conventional gas sensors often exhibit an unwanted response to gases or vapours other than the one it is desired to monitor. This cross-sensitivity to contaminants is considerably reduced when using correlation spectroscopy.

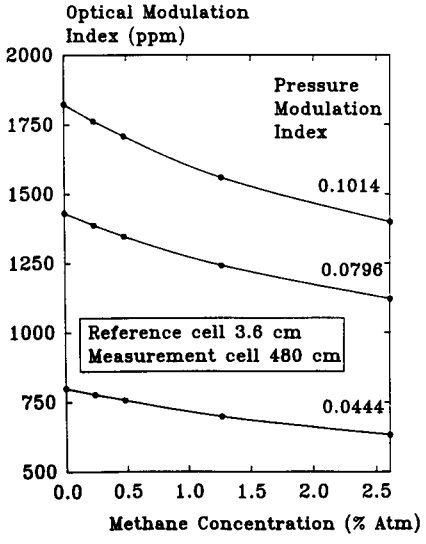

Fig. 6. Calibration curves for the pressure-modulated methane sensor showing optical-modulation index against measurement cell concentration.

The response of our methane sensor using the pressure-modulation method was experimentally determined for a number of contaminant gases and vapours. The numerical data are presented in Table 1 for various gases and vapours, including methanol, ethanol, ethane, dichloromethane and carbon dioxide.

A figure of merit, FOM, is defined; it is a measure of the improvement in cross-sensitivity of the pressure-modulated system compared with conventional gas-sensing techniques based on a simple measurement of mean absorption of the gas sample. Taking an optical modulation index, M, and a static fractional absorption, A, then the figure of merit was defined as $\{\Delta M(\text{methane})/\Delta M(\text{contaminant})\}/\{A(\text{methane})/A(\text{contaminant})\}$. The change in modulation index, ΔM, is given by the difference in index when the measurement cell is empty and when filled with the appropriate gas.

A typical contaminant such as ethane, which has a strong overlap with the methane spectrum, has a figure of merit around 30. As ethane is a likely contaminant in naturally occurring methane, this cross-sensitivity enhancement represents a useful improvement over conventional optical systems. As would be expected, gases with little spectral overlap with methane, such as carbon dioxide, register very little cross-sensitivity.

Stark-modulation gas detection

In the Stark-modulated scheme (Fig. 7), a large alternating electric field is applied to the gas in the reference cell in order to modulate its absorption spectrum. This results in a broadening of the absorption lines of the gas, hence varying the spectral overlap integral between the absorption spectra of the sample and reference cells, and causing a synchronous modulation of the detected signal. Correlation spectrometry using the Stark effect is attractive, because it results in a gas sensor with very simple hardware, and so could produce a low-cost system with good gas selectivity.

For the Stark technique to be viable, a gas molecule with a permanent electric dipole moment is essential. Fortunately, many important gases, such as water vapour, ammonia, hydrogen chloride, carbon monoxide and many oxides of nitrogen and sulphur have both suitable dipole moments [16] and absorption [17] properties. An additional requirement for efficient Stark modulation is for the gas absorption lines to be narrow (typically a few GHz), to ensure that significant modulation of the linewidth occurs under the action of the applied electric field.

TABLE 1. Cross-sensitivity data for the pressure-modulated methane detector

Sample gas	Path length (cm)	Gas conc. (atm)[a]	Fractional static absorption (%)	Modulation-index change (%)	Cross-sensitivity figure, FOM
Methanol	480	—[a]	−14.2	+0.50	119
	480	—[a]	−5.8	+0.22	110
	480	—[a]	−3.2	+0.08	159
	10	Sat. vap 19 °C	−3.5	+0.24	60
Ethanol	480	—[a]	−7.0	+0.75	39
	480	—[a]	−4.3	+0.51	36
	10	Sat. vap 21 °C	< 0.1	< 0.1	
Water	480	Sat. vap 22 °C	−0.3	−0.04	31
Ethane	480	—[a]	−15.1	+1.9	34
	480	—[a]	−14.9	+2.0	32
	480	—[a]	−10.7	+1.6	28
	10	100%	−11.5	+1.3	35
Dichloromethane	480	—[a]	−13.5	+3.4	17
	480	—[a]	−11.7	+3.0	16
	480	—[a]	−7.2	+1.2	24
	480	—[a]	−4.4	+1.0	18
	10	Sat. vap 22 °C	−9.3	+1.4	27
Carbon dioxide	480	100%	< 0.1	< 0.1	
Methane	480	1.27%	−3.2	−13.4	1
	10	100%	−5.2	−21.1	1

[a]Concentrations not measured, but can be inferred from static absorption measurement.

Stark modulation is a well-known physical phenomenon and is an established technique [18, 19] in the field of spectroscopy for the assignment of absorption lines. However, we have recently reported its first use for remote gas detection [20].

Spectroscopic aspects of Stark modulation

Any molecule that possesses a permanent electric dipole due to its atomic configuration will interact with an external electric field. The field causes the rotational energy levels of the molecule to split and shift via the Stark effect, although at NTP, the lines are generally broadened. Ammonia gas, for example, has a strong dipole moment, and hence Stark splitting of its energy levels is pronounced.

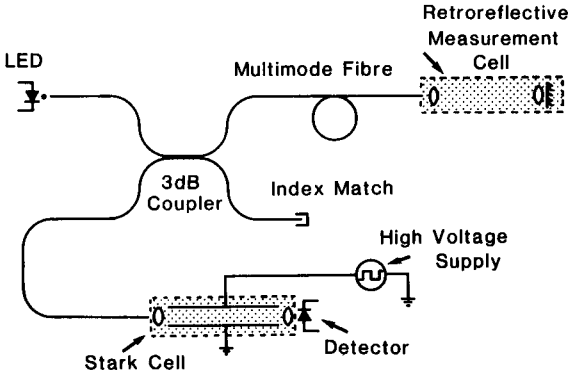

Fig. 7. Experimental configuration for the Stark-modulated ammonia detector.

Each individual absorption 'line' within the band is actually composed of a manifold of lines, which is effectively pressure broadened into a single line at atmospheric pressure. As the electric field is applied to the gas, many energy transitions are no longer degenerate and the lines split and separate further, resulting in line broadening from the already atmospheric-pressure-broadened line.

The absorption spectrum of ammonia at 1.5 μm is complex and irregular (Fig. 8) as it is formed from the overlapped spectra of two molecular vibrations. Consequently, theoretical modelling of the Stark effect is much more involved than for the other methods, and has not yet been performed.

The operation of the Stark-modulated gas detector can be described as follows. When no gas is present in the measurement cell, the detected signal level depends on the total absorption of the gas within the Stark cell. Ideally, for weak absorption lines, no change in the integrated transmission across the band is observed when the electric field is applied, as the lines are merely

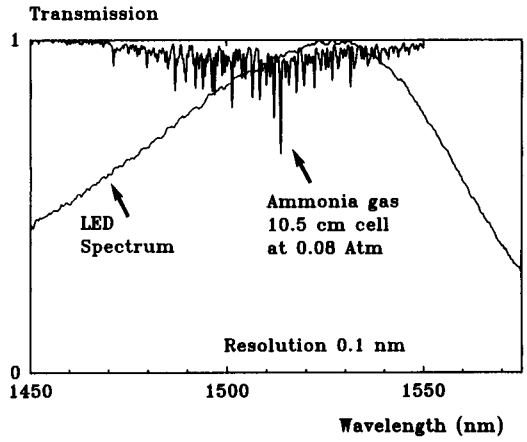

Fig. 8. Transmission spectrum for ammonia gas and emission spectrum for the light-emitting diode.

broadened and their effective absorption remains essentially unchanged. Consequently, the alternating component of the detected signal is close to zero with the measurement cell empty. In practice, however, a small modulation is observed, as the cell transmission, and hence the detected signal amplitude, has a non-linear dependence on the gas absorption coefficient.

As gas is introduced into the measurement cell, additional absorption is incurred due to this gas. If the latter is of the same species as the reference gas, then both sets of absorption lines will correspond. As the Stark field is applied, the effective transmission changes, due to a variation in the overlap integral of the absorption spectra. An alternating signal is detected which increases in magnitude with the concentration of the gas in the measurement cell. Any gas with absorption lines that do not overlap those of the reference gas will not produce a significant alternating signal, as the regions of the spectrum modulated by the Stark cell remain unaffected by the sample gas absorption. As with the pressure-modulation system, the detected signal is normalized by division by its mean value to provide a modulation index.

Experimental results for Stark modulation system

Initial results on Stark modulation [20] were performed with ammonia gas. A retroreflective measurement cell was employed with a two-way path of 40 cm. The arrangement allows use of a single fibre link to the sampling head and facilitates alignment. The reference cell had an optical path length of 20 cm between the plane-parallel electrodes. The Stark cell was driven by an electric field which alternated from zero to 840 kV m^{-1} at a 1 kHz rate. This value of electric field was below, but close to, the breakdown strength of the gas.

A 1.5 μm light-emitting diode, launching a power of 15 μW into the fibre, was employed as the optical source. The measured output spectrum of the device is given in Fig. 8, together with the absorption band for an ammonia gas sample.

The variation in the optical-modulation index was recorded as a range of ammonia concentrations was introduced into the measurement cell. The calibration curve of optical-modulation index against measurement cell concentration of ammonia is given in Fig. 9, at a Stark cell concentration of 0.07 atm. A positive response to ammonia was exhibited, and, as expected, the optical-modulation index was observed to increase with measurement cell gas concentration. The slope of the curve diminishes at higher concentrations, as the gas in the measurement cell begins to absorb a significant fraction of the light within each absorption line, and the stronger lines, in particular, become saturated. A small offset in modulation index is exhibited at zero measurement cell concentration. This is due to the fact that, for stronger absorption lines within the band, a difference in the integrated transmission occurs when they are subjected to a Stark field because of the non-linear nature of absorption.

The sensitivity of the system to ammonia can be determined from the data presented in the Figure. The ultimate sensitivity is taken as the value for unity signal-to-noise ratio. A noise-limited sensitivity of 0.0016 atm (or 0.16% by volume) ammonia, for a 10 s measurement time constant, was determined for the present system. Alternatively, this can be presented as an absorber amount, giving a sensitivity of 0.064 atm cm. Extrapolating this result to the longer sensing path length of 480 cm used for the pressure-modulation system results in a predicted sensitivity of approximately 130 ppm ammonia.

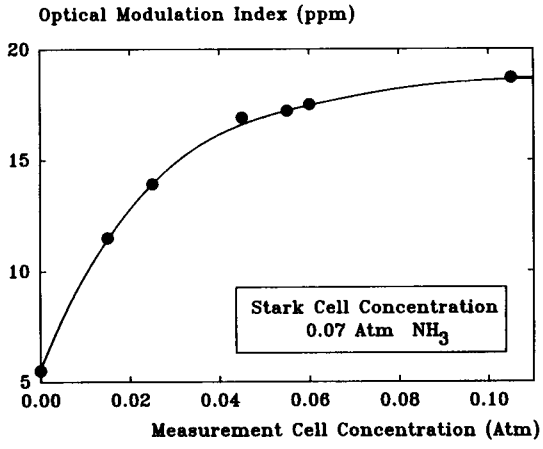

Fig. 9. Measured optical-modulation index vs. measurement cell concentration for the ammonia detector.

Phase-modulation gas detection

Modulation can be achieved by an indirect method by redistribution of the optical spectrum of the light as it passes between the measurement and reference gas cells. A schematic diagram of this modulation technique is given in Fig. 10. A frequency- or phase-shift modulation device is included in the optical path between the cells in order to effect a deliberate spectral translation or 'broadening' of the spectral lines.

Phase-modulation correlation spectrometry employing bulk optics was first demonstrated by Rider *et al.* [21] and used to detect nitrous oxide in the upper atmosphere. As the gas pressures employed were low, the intrinsic linewidths were small, typically 0.6 GHz, and a modulator with only a modest performance was adequate. For the current application a high-performance phase modulator is essential. In this paper, we report the first example of gas sensing using this method at atmospheric pressure. Here, absorption linewidths are considerably greater due to pressure broadening and are typically in the range 3–5 GHz. In addition, optical fibre links are employed in our work, which allow the gas-sampling head to be remotely monitored from a base station.

In common with the other methods of correlation spectrometry, phase modulation provides a gas sensor with excellent selectivity to the desired gas. Also, the technique may be applied to any gas species, provided that the absorption spectrum comprises narrow distinct lines in a suitable region of the wavelength spectrum.

Phase modulators for gas detection

An electro-optic crystal can perform phase modulation of light by exploiting the linear electro-optic effect, whereby a change in optical delay is induced in proportion to the applied electric field. By sinusoidally varying the refractive index, and hence modulating the phase of the light, each wavelength component of the transmitted energy is split into a series of sidebands.

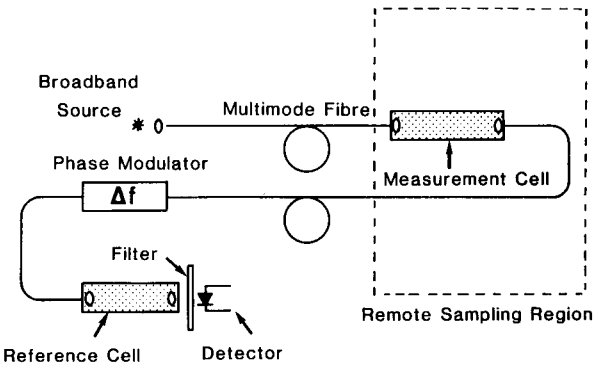

Fig. 10. Schematic diagram of the experimental configuration for the angle-modulated scheme.

Two types of phase modulator were employed for the experimental investigation here, both formed from lithium niobate. The first was a bulk-optic device, comprising a 36.5 mm length of crystal with a 1 mm × 1 mm section and electrodes on the Z-faces. Light from a multimode fibre was collimated with gradient index lenses, and propagated along the major dimension (Y axis) of the modulator crystal. At a drive frequency of 426 MHz, the phase deviation was estimated to be 0.85 radians at 1.6 μm wavelength for the Z-polarization. In operation, the modulator had a fibre-to-fibre insertion loss of 2.5 dB.

The second electro-optic device was a commercial packaged phase modulator with single-mode fibre tails, primarily intended for communication purposes [22]. The integrated optic device within the package comprised a single-mode optical waveguide channel formed in the lithium niobate substrate. The insertion loss was large ($\sim$27 dB) when this single-mode device was employed in a gas-sensing system using multimode fibres. However, the device was capable of producing a much larger phase deviation, estimated from manufacturer's data to be 3.5 radians, at a high frequency of 2.7 GHz.

Effects of phase modulation

Phase modulation can be considered to disperse each monochromatic component of the incident optical spectrum into a number of sidebands. As predicted by conventional phase-modulation theory, the sideband spacing is equal to the modulation frequency. The intensity of each sideband is determined by Bessel functions and is dependent on the magnitude of the phase deviation.

As with all the other methods, a change in the detected optical signal is measured as a small modulation on the mean optical level. This results from a difference in the integrated transmission of the system where the phase modulator is periodically activated. When gas is present only in the reference cell, no signal is expected at the receiver because the action of the phase modulator is merely to redistribute the flat optical spectrum exiting from the empty measurement cell. Clearly, this has no observable effect on the net integrated transmission. However, upon introducing gas into the measurement cell, a modulation of the detected optical level is expected, as the optical spectrum input to the phase modulator is now no longer flat, due to the presence of the absorption lines of the gas sample. When the phase modulator is activated to redistribute the frequency spectrum, there is a variation in the overlap integral between the absorption bands of sample and reference gas spectra, which gives rise to a modulation in the total transmission.

When the spectra do not overlap, as would be the case with different gas species in measurement and

reference cells, then the signal recorded is extremely small. This requirement for precise overlap of absorption lines, in order to register a signal, ensures that the method is highly selective. This is particularly true when the gas to be measured has a large number of fine lines in its absorption spectrum.

Theoretical analysis of the phase-modulation method

In order to analyse the performance of the phase-modulated gas-detection scheme, a simplified model based on the treatment of a single absorption line of the gas band is assumed. This approach is a good approximation for gas species having many separate regularly spaced absorption lines, such as methane and carbon dioxide, but results for a more irregular band may prove to be less satisfactory.

As with the pressure-modulation method, the optical transmission is calculated by performing integration over an optical frequency interval v_1 to v_2, equivalent to the line spacing within the band, with the gas line centred within the integration span. The lineshape chosen for our analysis is again that proposed by Lindholm.

The optical signal ΔI can be calculated from the model as a function of gas concentration in the measurement cell. As the drive to the phase modulator is periodically activated, a change in the integrated transmission results:

$$\Delta I = I_0 \int_{v_1}^{v_2} T_2(v)\left[T_1(v) - \sum_{i=-\infty}^{\infty} T_1(v - if_m)J_i^2(\delta)\right]\delta v \quad (3)$$

The optical spectral density at the receiver with both reference and measurement cells empty is represented by I_0. The phase modulator has a modulation frequency f_m, and $J_i^2(\delta)$ is the intensity of the ith sideband, where δ is the peak phase deviation. The mean optical power level I_{mean} transmitted through the system can be calculated from

$$I_{mean} = I_0 \int_{v_1}^{v_2} T_1(v)T_2(v)\delta v - \Delta I/2 \quad (4)$$

The optical modulation index $\Delta I/I_{mean}$ can thus be calculated for linestrengths representative of weak (e.g., P9), moderate (e.g., P6) and strong (e.g., R6) absorption lines of the $2v_3$ methane band. The linestrengths were estimated [11, 12] to be 1.245, 2.867 and 6.604 $atm^{-1} cm^{-1} GHz$ for the P9, P6 and R6 lines, respectively. As two different types of electro-optic phase-modulator devices were employed for the experiments, the theoretical modelling was performed using the phase deviation and modulation frequency values appropriate for each case.

The optical-modulation index was calculated as a function of measurement cell length, and results of the simulation are presented in Fig. 11. The path length of the reference cell was chosen to coincide with the experimental value of 5.7 cm. The phase modulator was assumed to have a phase deviation of 0.8 radians at a drive frequency of 400 MHz; a value chosen to be close to the practical value for the bulk optic modulator employed for the experiments. The response plotted for each of the three linestrength values, corresponding to the P9, P6 and R6 lines, shows the expected increase in optical-modulation index as the measurement cell length is increased.

A similar theoretical system response plot is given in Fig. 12, again showing the expected variation in optical-modulation index with measurement cell length. The same parameters are assumed for this simulation, except that a phase deviation of 3.5 rad at a frequency of 2.68 GHz was chosen. These values correspond to

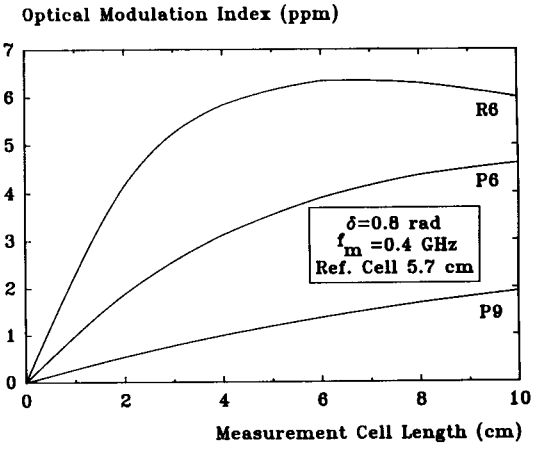

Fig. 11. Calculated optical-modulation index vs. measurement cell length for the bulk-optic phase-modulator case.

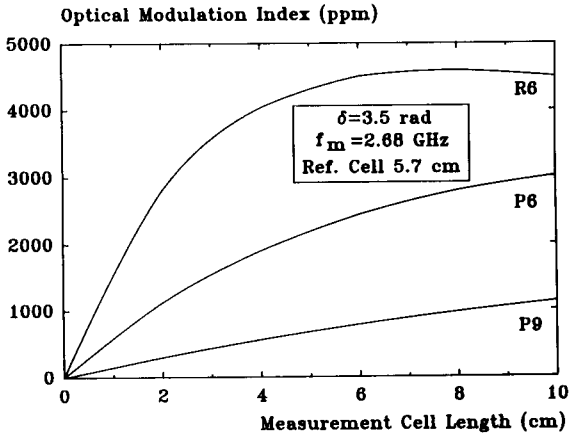

Fig. 12. Calculated optical-modulation index vs. measurement cell length for the integrated-optic phase-modulator case.

the single-mode integrated-optic modulator used for the latter part of the experimental investigation.

Experimental results

The optical configuration shown in Fig. 10 was employed for an experimental investigation of the phase-modulated gas-detection scheme. The system was evaluated with methane gas, using a filter of 50 nm linewidth to select the $2\nu_3$ methane band centred at 1.67 μm. The reference cell had a 5.7 cm path, and was filled with methane at 1 atm (100%) concentration. A number of measurement cells were employed with lengths up to 10.5 cm, but all containing 1 atm (100%) methane. In this case it was convenient to vary the measurement cell length, rather than the concentration, in order to achieve a range of equivalent absorber amounts.

Initial experiments were performed with the bulk-optic modulator and multimode (100/140 μm) fibre links. The r.f. modulator drive was periodically interrupted at a 10 kHz rate and the optical signal was synchronously detected with an integration time constant of 10 s. The experimental results achieved with this modulator using a 10.5 cm measurement cell are shown in Fig. 13, as the measurement cell was repeatedly filled with methane and flushed with nitrogen.

For the second phase of the experiments the integrated-optic phase modulator was substituted for the bulk-optic device. In this case, light from the broadband source was launched through the measurement cell and then directed into the single-mode fibre pigtail of the modulator. The modulator optical pigtail was spliced onto the remainder of the multimode optical network, which was unchanged from the bulk modulator configuration.

The drawback with the integrated-optic modulator is the low overall transmission achieved, due, first, to the poor coupling efficiency from the broadband source into the single-mode fibre tail and, secondly, to the high intrinsic loss (8 dB) of the modulator itself. Consequently, the power received at the detector measured only 280 pW, which was 27 dB less than that achieved with the bulk modulator.

A plot of optical-modulation index measured over a range of measurement cell lengths is given in Fig. 14 for the integrated-optic modulator. An offset of 2800 ppm in the optical-modulation index was observed at zero measurement cell gas concentration, which was subtracted from the true signal in order to generate the plot. The offset was attributed to extraneous optical amplitude modulation occurring within the phase modulator. In order to attain stability of the signal, it was found to be necessary to control the temperature of the modulator.

The detection sensitivity for methane achieved with the integrated-optic modulator can be calculated from

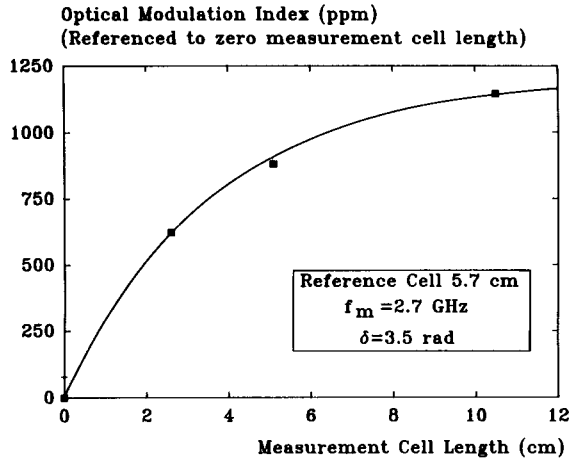

Fig. 14. Measured optical-modulation index vs. measurement cell length for the integrated-optic phase modulator.

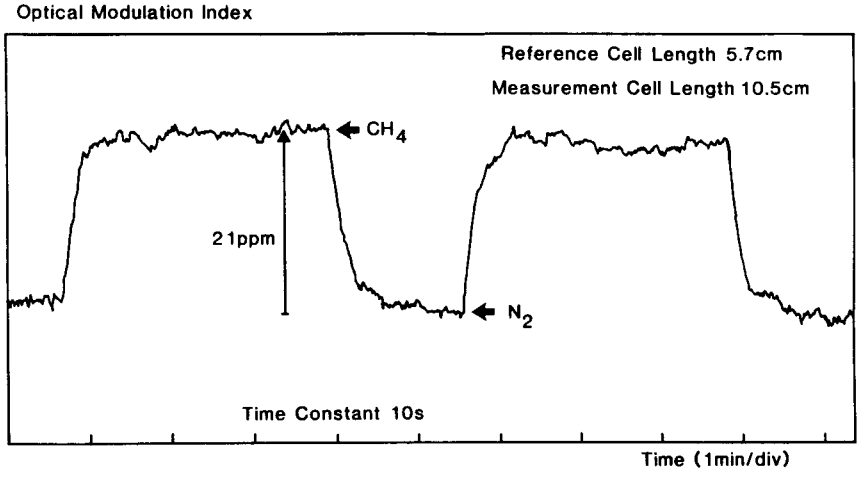

Fig. 13. Measured optical-modulation index vs. time for the bulk-optic phase modulator as the measurement cell is filled with methane.

the data presented in Fig. 14, assuming a signal-to-noise ratio limit of unity. The sensitivity, expressed in normalized units of absorber amount, was found to be 0.134 atm cm for a 10 s measurement time constant. On extrapolating the absorber amount to a longer path length of 500 cm, a noise-limited sensitivity of approximately 300 ppm methane by volume is anticipated. It should be noted that this level of performance is predicted despite the rather poor detector signal-to-noise ratio, which arose as a result of using the high-loss single-mode modulator with a low-radiance source. Considerably improved results are expected using higher-radiance sources and a lower-loss phase modulator.

Conclusions

We have reviewed earlier work on real-time correlation spectroscopy using pressure- and Stark-modulation schemes. The methods can be used to construct highly selective gas detectors employing broadband sources. In addition, we have reported the first atmospheric pressure results for an indirect scheme, using electro-optic modulation between gas cells. We have presented our theoretical models for the pressure- and phase-modulation methods, based on a Lindholm lineshape, and found good agreement with experimental results.

All the methods reported have different attractions, depending on their intended application, and form a generic set of complementary gas-sensing methods which have excellent cognitive behaviour.

References

1 P. C. Hills, P. J. Samson and I. Webster, Explosion hazards of optical fibres in combustible environments, *Proc. 7th Optical Fibre Sensors Conf., Sydney, Australia, 1990*, p. 63.

2 N. P. Ludlam, Safety of optical systems in flammable atmospheres, *Report for Optical Sensors Collaborative Association, UK, R/1008/00/A*, 1989.

3 A. Hordvik, A. Berg and D. Thingbo, A fibre optic gas detection system, *Proc. 9th European Conf. Optical Commun., Geneva, Switzerland, 1983*, p. 317.

4 T. Kobayashi, M. Hirana and H. Inaba, Remote monitoring of NO_2 molecules by differential absorption using optical fibre link, *Appl. Opt., 20* (1981) 3279.

5 R. Goody, Cross-correlating spectrometer, *J. Opt. Soc. Am., 58* (1968) 900.

6 F. W. Taylor, J. T. Houghton, G. D. Peskett, C. D. Rogers and E. J. Williamson, Radiometer for remote sounding of the upper atmosphere, *Appl. Opt., 11* (1972) 135.

7 H. O. Edwards and J. P. Dakin, A novel optical fibre gas sensor employing pressure-modulation spectrometry, *7th Optical Fibre Sensors Conf., Sydney, Australia, 1990*, p. 55.

8 A. R. Curtis and R. M. Goody, Spectral shape and its effect on atmospheric transmission, *Q. J. R. Meteorol. Soc., 80* (1954) 58.

9 H. Margenau and W. W. Watson, Pressure effects on spectral lines, *Rev. Mod. Phys., 8* (1936) 22.

10 L. L. Beranek, *Acoustics*, Acoustical Soc. Am., 3rd edn., 1986.

11 J. S. Margolis, Measured line positions and strengths of methane between 5500 and 6180 cm^{-1}, *Appl. Opt., 27* (1988) 4038.

12 R. Partridge, UK National Physical Laboratory, personal communication, Oct. 1988.

13 L. S. Rothman *et al.*, The HITRAN database: 1986 edition, *Appl. Opt., 26* (1987) 4058.

14 L. Darnton and J. S. Margolis, Temperature dependence of the half widths of some self- and foreign-gas-broadened lines of methane, *J. Quant. Spectrosc. Radiat. Transfer, 13* (1973) 969.

15 J. U. White, Long optical paths of large aperture, *J. Opt. Soc. Am., 32* (1942) 285.

16 *Handbook of Chemistry and Physics*, CRC Press, Boca Raton, 68th edn., 1987.

17 T. Y. Wu, *Vibrational Spectra and Structure of Polyatomic Molecules*, Edwards, Ann Arbor, MI, 1946.

18 G. D. Barrow, *An Introduction to Molecular Spectroscopy*, McGraw-Hill, New York, 1972.

19 C. N. Banwell, *Fundamentals of Molecular Spectroscopy*, McGraw-Hill, New York, 1972.

20 J. P. Dakin and H. O. Edwards, Progress in fibre-remoted gas correlation spectrometry, *Proc. ECO4, Int. Congress Optical Sci. Technol., The Hague, Netherlands, 1991.*

21 D. M. Rider, J. T. Schofield and J. S. Margolis, Electrooptic phase modulation gas correlation spectroscopy: a laboratory demonstration, *Appl. Opt., 25* (1986) 2860.

22 Lithium niobate phase modulator-type IOC1000, *BT&D Technologies Tech. Bull.*, Ipswich, UK.